Fracturing of rock ahead of the face of an excavation and its relevance to mechanized excavation

by M. Mokgohloa[1] and T.R. Stacey[2]

Affiliation:
[1]Department of Mineral Resources and Energy, University of the Witwatersrand, South Africa
[2]School of Mining Engineering, University of the Witwatersrand, South Africa

Correspondence to:
T.R. Stacey

Email:
Thomas.Stacey@wits.ac.za

Dates:
Received: 17 July 2023
Revised: 7 Nov. 2023
Accepted: 17 Sept. 2024
Published: November 2024

How to cite:
Mokgohola, M. and Stacey, T.R. 2024. Fracturing of rock ahead of the face of an excavation and its relevance to mechanized excavation. *Journal of the Southern African Institute of Mining and Metallurgy*, vol. 124, no.11 pp. 653–660

DOI:
http://dx.doi.org/10.17159/2411-9717/2966/2024

ORCiD:
T.R. Stacey
http://orcid.org/0000-0003-3763-9193
M. Mokgohola
http://orcid.org/0009-0006-6932-008X

Abstract

Boring of tunnels and shafts in hard rock under high stress conditions is becoming more common as mines and tunnels are developed at greater depths. Under the high stress conditions, fracturing of the often-brittle rock occurs in the walls, backs, and ahead of advancing faces of excavations. Fracturing can have a significant impact on boring activities: sidewall spalling, which affects machine gripper capacity, and fractures can also develop in the rock ahead of the face, leading to blocky rock conditions, which may have a significant effect on machine excavation. Fracturing may develop dynamically, leading to rock bursts manifesting in the form of strain bursts, which can be hazardous and destructive. In brittle rock, fracturing is commonly extensional in nature. The focus of this paper is on fracturing in the face of the excavation. Examples of such fracturing behaviour are described briefly in the paper. Numerical analyses were carried out to predict the initiation of extension fractures and their orientations ahead of excavation surfaces, and the resulting formation of rock slabs/plates, and the stability of these plates. The results should be beneficial for the evaluation of the conditions prior to, and during boring operations.

Keywords

rock fracture, extension strain, tunnel boring, raise boring, strain burst

Introduction

Mines are operating at ever greater depths and therefore, access tunnels, shafts, and other excavations must be developed under very high stress conditions. In the civil engineering industry, tunnels are now also being developed under very deep cover for transport and hydroelectric purposes. As a result, the rock surrounding the excavations is subjected to very high stresses, leading to fracturing, spalling and, in some cases, rock bursting. Owing to the hazardous conditions, mechanized excavation methods are increasingly being used in the mining environment, and tunnel boring is commonly used for civil tunnels. The fracturing, spalling, and rock bursting that occur pose significant challenges to these mechanized excavation methods. In this paper, cases published in the literature are summarized to indicate the typical rock fracturing that mechanized equipment, in particular boring machines, will encounter under high stress conditions.

Experiences during boring of excavations in high stress, hard rock conditions

There are numerous publications dealing with spalling and its prediction under high stress conditions (Martin et al., 1997; Steffanizzi et al., 2007; Barla, 2014; Vazaios et al., 2019a; Vazaios et al., 2019b; Feng et al., 2018). In this section, brief descriptions reported in the literature will be given of cases of fracturing of brittle rock associated with boring under high stress conditions.

In the 1970s an open face 3.36 m diameter tunnel boring machine was introduced into a gold mine in South Africa, for the purpose of tunnel development at a depth of 2000 m (Graham, 1976). Shortly after the boring operation commenced, problems were encountered that severely limited the progress of the boring machine. These included 'spalling of rock from the sidewalls, which in some cases was so extensive that the machine grippers could not reach the sidewalls; fall-out of blocks of rock from the face; abnormally high cutter wear, which resulted from inadequate gripping owing to fracturing of the sidewalls; damage to the belt conveyor caused by sharp pieces of fractured rock; accumulation alongside the machine of rock debris, which was hand lashed and resulted in delays.' (Stacey and De Jongh, 1977). An investigation and analysis of the problems were carried out, involving mapping of the extent and orientation of stress-induced fractures around the tunnel and ahead of the face. This showed that all fractures observed were tensile, with clean surfaces, and there was no evidence of crushed material that would indicate shearing. Barring of the face

revealed slabs 10 to 30 mm in thickness that were curved with the same radius as the cutter head. This confirmed the observation by borehole periscope of a fracture ahead of the face.

Problems were also experienced with another tunnel boring trial in a different gold mine (Taylor et al., 1978; Burgess and Taylor, 1980). This was a 3.4 m open face machine with two grippers on each side. After seven months of boring over a length of 196 m, major machine alterations were required, owing to the occurrence of rock fracturing (Taylor et al., 1978). The tunnel face came away in relatively large blocks, which measured around 0.6 m by 0.4 m by 0.3 m. These caused the head to jam, continually damaging the front transfer chute. Word of mouth also indicated that, to replace cutters (from the front), the machine had to be retracted several metres, since rocks popped somewhat violently from the face, causing hazardous conditions.

Fracturing at the face of a bored Alpine tunnel, which appears to be similar to the one described by Taylor et al. (1978), which was further described by Kaiser (2006), referring to Weh and Bertholet (2005). Experiences in other Alpine tunnels are described by Loew et al. (2010). During the construction of the Lötschberg base TBM tunnel with a cover of approximately 2000 m, spalling and bursting were experienced, mainly in front of the machine. In some instances, this involved the violent ejection of rock blocks, to the extent that the TBM cutter head vibrated for several minutes. Substantial energy release in the form of a strain burst was experienced (Kaiser et al., 1996).

Descriptions of rock burst, spalling and slabbing failures during construction of a hydropower station are given by Gong et al. (2012) and Feng et al. (2018). The overburden cover along the headrace tunnels is greater than 1500 m over much of its length, with a maximum cover of 2525 m. Rockbursts were experienced during excavation of the tunnels. Gong et al. (2012) refer to tunnel boring machine (TBM) cutterhead seizure due to rock bursting at the face, and the substantial time taken to clear rock debris in such a case. They also deal with the effects of rock bursting on cutter wear and cutterhead failure: the slabbing and rock bursting leading to an uneven face, impact loading, and cutterhead vibrations. The slabbing and irregular blocks resulting from rock bursting also caused problems with muck removal and damaged the belt conveyor. Zhang et al. (2012) also described major problems associated with rock bursting during tunnel development. However, these were associated with drill and blast excavation, not TBM excavation.

During raise boring at depth, many problems associated with rock fracturing have been experienced and large slabs of rock, with side lengths exceeding a metre, were frequently seen at the cutter head (Stacey and Harte, 1989). Hern and Engelsman (1988) reported problems associated with raise boring: 'The bit body lost penetration. The bit body was lowered and found to be completely compacted. Large boulders fell from the cutting face and became trapped between the cutter wings and the stabilizer wings.' Almost identical behaviour was described more recently by Rojat et al. (2009): 'The boulders which led to packing problems also caused great concern for the miners' safety when servicing the equipment… A large boulder fell and bent one of the pipes… This canopy was also damaged when a large boulder fell… Bit body was put back into service and reamed an additional 50 metres at which time the first stabilizer failed, allowing the bit body to fall 125 metres.'

Small diameter raise boring as a method of mechanized mining has been trialled in gold mines in South Africa. Early trials experienced fracturing of the rock at the face, as illustrated in Figure

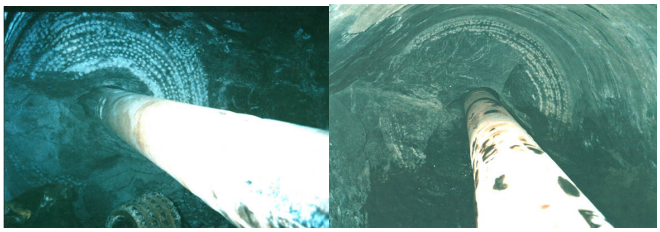

Figure 1—Raise boring of reef in a gold mine, showing fracturing of the face and damage to cutters (photographs provided by W. D. Ortlepp)

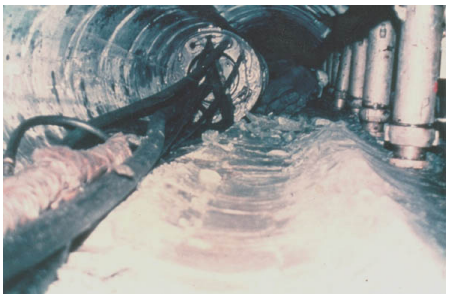

Figure 2—Stope coring of gold reef

Figure 3—Exposed face of a stopecorer hole

1. More recent trials with this method are described by Roberts (2017). However, he focuses on the sidewall breakouts in the holes and does not mention fracturing of the face of the bore.

During experimental mechanized mining of gold reef by stope coring (Stacey, 1982b), shown in Figure 2, it was found that the rock being cored 'burst' spontaneously within the 600 mm diameter core barrel.

Figure 3 shows the face of a Stopecorer hole after face bursting, exhibiting a clean extension fracture surface. During one of the phases of the experimental coring programme, about an hour after coring in the first hole to be drilled, a 'disc', involving the full diameter, suddenly 'burst' very audibly off the face. This occurrence correlates with the observation of a fracture occurring ahead of the face of the Atomic Energy of Canada Limited (AECL) tunnel described by Martin (1997).

On a much smaller scale than the stope coring, drilling of borehole core under high stress conditions often results in discing of the core, examples being shown in Figure 4.

The fractures in the core are almost certainly extension fractures and extremely unlikely to be shear fractures. Stress analyses of coring, assuming axisymmetric conditions (Stacey, 1982a), showed a zone of extension strain ahead of the coring (Figure 5), which corresponds with the fracturing in Figure 4.

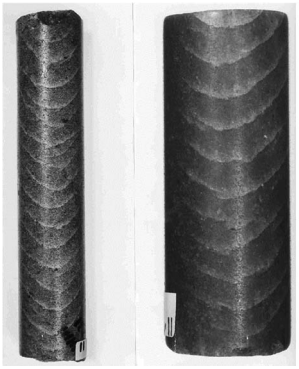

Figure 4—Incipient discing fractures in borehole core

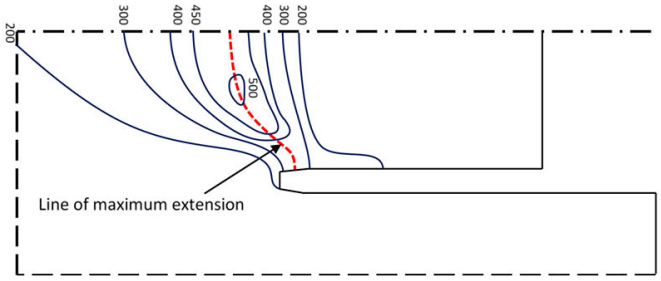

Figure 5—Analyses of potential core discing (Stacey, 1982a)

A relevant case, although not of a bored tunnel, involved the development of a drill and blast tunnel in a gold mine at a depth of 2800 m below surface (Ortlepp, 2001). After a blast to advance the tunnel, the tunnel self-mined a length of 16 m. This length formed along the line of a geological fault. The rock fragments resulting from the advance were similarly sized platelets 150 to 300 mm in size with a thickness of 0.1 to 0.2 times the diameter. The tunnel was partly filled with these fragments to a depth of 1.5 m, for a distance of 50 m from the blasted face. Release of occluded gas was associated with the event. Ortlepp (2001) suggested the following mechanism: 'Extension fractures developed in the rock immediately ahead of the face. These would be sub-parallel to the face, forming thin slabs'; 'The thin slabs or plates buckled under the high stress and burst outwards (ejection). In buckling, the slabs/plates broke into smaller fragments, which explains the size of platelets and the fines observed.' Simple numerical stress analyses, using an extension strain failure criterion, indicated that a zone of extension strain occurred ahead of the tunnel face, and that the formation of the 'cavity' would follow the fault line.

It is apparent that the prediction of rock fracturing is critical for the evaluation of failure around excavations. The examples given indicate that extension fracture and failure are predominant in the high stress, brittle rock conditions encountered at deep levels. Van Aswegen (2013) states that, regarding fracturing of rock in a deep level gold mining environment, 'The most commonly observed mining induced structures are extension fractures'. Barton and Shen (2017a) and Barton and Shen (2017b) describe extension failure in many competent rock conditions. The extension strain criterion (Stacey, 1981; Wesseloo and Stacey, 2016) for predicting fracturing and failure appears to be beneficial in this regard. The criterion predicts failure, even in areas of low stress magnitudes (Stacey and Yathavan, 2003), which occurs when total extension strain in the rock exceeds a critical value characterizing the rock type. The examples described in the afore-mentioned give a clear indication of the impact of extension fractures on the boring operations, ranging from spalling to buckling and even to bursting. Knowledge of the extent of potential fracturing will be beneficial to the boring projects, in particular when using tunnel boring machines, which may be susceptible to rock fracturing and rock bursting.

The above case studies demonstrate the detrimental effects that spalling of rock from the face and sidewalls of bored tunnels, shafts, and raises can have on the boring process. The implications are that the cutter head may encounter slabs and blocks of rock in the face that could be large. This will lead to uneven rotation, high cutter wear and irregular torque demand, all of which will affect the efficiency of the boring. Large blocks may also clog the cutter head and cause damage to the transfer chute and conveyor belt. In extreme conditions, strain bursting from the bored face may occur, with potentially destructive consequences. Fracturing and breakouts in the walls of the bore will be locations of impact on, and therefore wear and damage to gauge cutters. They will also result in uneven and loosened surfaces for machine grippers.

It is clear from many of the cases described that fracturing in a hard rock environment is extensile. Many descriptions of the fracturing involved refer to extension fractures. As a result, in this paper, the focus is on the face of the bore, and on the prediction of extension fracturing and spalling from the face that could occur in strong, brittle rock under high stress conditions. Wesseloo and Stacey (2000) evaluated zones of extension strain exceeding a typical critical magnitude surrounding, and ahead of, the face of a tunnel for a range of three dimensional in situ stress conditions (Figure 6). Such zones could certainly influence the performance of tunnel and raise boring, the further development of instability in the rock, and hence, the rock support requirements in the tunnel.

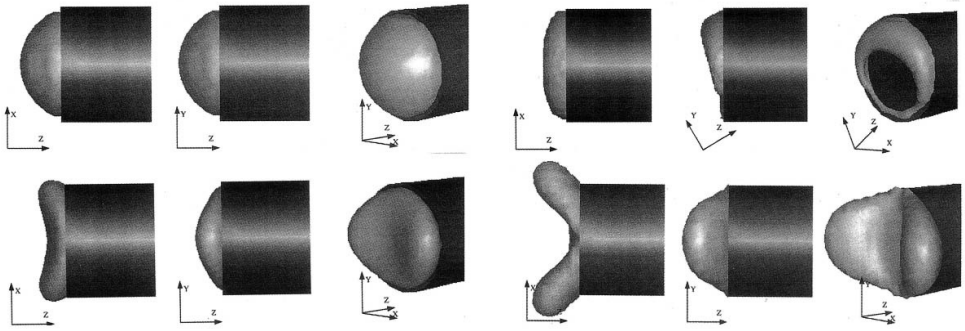

Figure 6—Zones of extensional strain exceeding 200 microstrain ahead of a tunnel face under a range of three dimensional in situ stress conditions (Wesseloo and Stacey, 2000)

A further example is the well-published AECL tunnel in Canada (Martin et al, 1997), which, although not a bored tunnel, did not involve excavation by blasting. This is a high-quality case study since the parameters are well known: the rock strength parameters and the in situ stresses, as well as the history of fracture and failure development. Breakout development was modelled using alternative failure criteria. The observed breakout geometry was matched well using the cohesion weakening friction strengthening criterion (Hadjiabdolmajid et al., 2002), as shown in Figure 7, but this also indicated failure on the sub-horizontal axis, which did not occur. The Mohr-Coulomb prediction was completely incorrect. Wesseloo (2000) modelled the development of the breakout, using a finite difference numerical analysis stepwise approach, applying an extension strain criterion (Wesseloo and Stacey, 2000). Zones adjacent to the surface, indicated as failed after each step, using the criterion, were nulled to simulate fallout of spalling rock. The predicted development of the breakout eventually stabilized, and its final geometry matched the observed geometry, as shown in Figure 7.

Criticism of this stepwise process could be levelled because of the 'manual' interaction, and because of the assumption of plane-strain conditions. However, it is important to consider the three-dimensional stresses. The axial stress magnitude, which may be different from that in the plane-strain assumption, has a significant influence on breakout formation (Xiang et al., 2023). However, the results of the analyses indicate the validity of the extension strain criterion, and further support in this regard is provided by Steffanizzi et al. (2007). This AECL example demonstrates the importance of using an appropriate failure criterion that corresponds with the expected failure mechanism. It is also important to note that, during development of this tunnel (Martin, 1997), microseismic events were recorded ahead of the tunnel face, indicating fracture development. In addition, it was noted that, after the drilling of the perimeter holes around the tunnel for mechanical excavation, a fracture formed ahead of the tunnel face (ISRM, 2012). Discrete fractures also occurred ahead of the face of the bored tunnel described by Stacey and De Jongh (1977).

In the stope coring example referred to, the bursting of the core was an obvious advantage from the point of view of production progress, since the rock was fragmented in the bursting process, allowing coring to be continuous. However, the problem that arose was one of the predictions of the conditions under which such bursting would, or would not, occur. This was dependent on the span of the stope created (the number of overlapping holes cored), which determined the stresses acting on the rock at the coring face. Some success was achieved with a simple analysis using an extension strain criterion (Stacey, 1982b). Figure 8 shows a series of diagrams in which the black shading indicates that the critical extension strain has been exceeded.

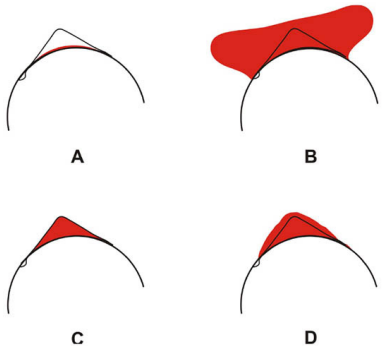

Figure 7—Failure extent predicted by alternative criteria. (A: observed geometry; B: Mohr Coulomb; C: Extension strain; D: Cohesion-weakening-friction- strengthening)

At a span of 4.6 m, equivalent to 9 Stopecorer holes, it is only the circumferential area in which the extension strain criterion is not exceeded. The encountered condition showed that bursting occurred from the 8th hole onwards, indicating a satisfactory agreement between prediction and practice.

As a result of the widespread observations of extension fracturing associated with tunnel boring and the spalling from the face, the focus of stress analyses described in the next section will involve the face region and the use of an extension strain failure criterion (Wesseloo and Stacey, 2016). This criterion is summarized as follows:

$$\varepsilon_3 = [\sigma_3 - \upsilon(\sigma_1 + \sigma_2)]/E \quad [1]$$

For failure, the criterion is: $\varepsilon_3 \geq \varepsilon_{cr}$

Where ε_{cr} is the critical value of extension strain. Applicable values can be determined from the uniaxial compressive strength, the modulus of elasticity and the Poisson's ratio of the rock, using the Equation [2]:

$$\varepsilon_{cr} = f.\ UCS.\ \upsilon/E \quad [2]$$

For fracture initiation strain, it is suggested that the value of '*f*' should be 0.3 and, for crack damage strain, the value of '*f*' should be 0.7. The orientation of the fracture (failure) surface will be normal to the direction of σ_3.

It is postulated that, owing to the three-dimensional stress field acting on the tunnel face geometry, extension fractures will be formed in the rock ahead of the face as the tunnel boring progresses. It is also postulated that fractures will coalesce to form slabs or shells immediately ahead of the face, and that their thickness will be determined by the thickness critical for buckling. Thus, the extent of fracturing and the orientation of the fractures will be determined using an extension strain criterion, and the potential thickness of the slabs/blocks formed due to the high stresses will be determined using buckling criteria.

Three-dimensional numerical stress analyses

Stress analyses around a bored excavation in rock with the assumed properties of quartzite, and for several in situ stress ratios and magnitudes, were carried out using RocScience's Examine3D program. The use of elastic analysis is justified, since the objective is to determine the potential failure extent at the onset of failure, and not to attempt to model actual failure, which will be in the non-linear mode. In addition, excavation involves *unloading*, normal to the surface of the excavation, which is likely to be initially elastic, or at least linear. The input parameters used for the analyses are summarized in Tables I and II.

Principal stress and extension strain distributions were evaluated. In these analyses, critical extension strain values, ranging from 180 to 270 microstrain for crack initiation, and from 504 to 864 microstrain for the crack damage (failure), were considered for the quartzite (Wesseloo and Stacey, 2016). To identify the geometry of potential slabs resulting from the fracturing, fracture orientations were determined from the analyses. Potential buckling of the

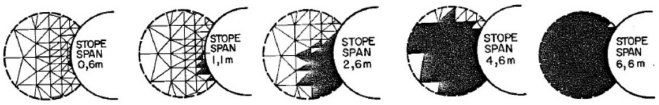

Figure 8—Predicted extents of Stopecorer face fracturing (Stacey, 1982b)

Table I

Typical input parameters for brittle rock such as quartzite

Parameters	
Elastic modulus	50 GPa
Poisson's Ratio	0.2 and 0.3
Uniaxial compressive strength	180 MPa

Table II

Alternative in situ stress fields considered. (x-axial; y-vertical normal; z-horizontal normal)

Stress (MPa)		
σ_x	σ_y	σ_z
70	35	70
35	35	70
52.5	25	70
35	17.5	52.5
52.5	70	25

slabs was then evaluated, based on fracture extents predicted for a critical extension strain of 200 microstrain. The results indicated similar principal stress distributions, under the same in situ stress conditions, around tunnels of different diameters. As would be expected, the predicted extents of failure vary for different tunnel sizes.

The relationships between the predicted maximum failure depths around an 8 m diameter tunnel and the critical extension strains are shown in Figure 9. This indicates the sensitivity of the in situ stress ratios and the critical extension strains. Both crack initiation and crack damage points are indicated on the graphs. As can be expected, since the analyses were elastic, there is a linear relationship between predicted depths of fracturing and values of the critical extension strain, and the tunnel size. This implies, confirming experience, that a smaller diameter tunnel is less likely to cause boring problems than a larger diameter tunnel.

For one of the in situ stress conditions, the potential extent of fracturing around and ahead of an 8 m diameter tunnel is shown as isosurfaces in Figure 10. From this figure, it can be seen that the tunnel face area is within a 'cocoon' of fractured rock. There are substantial zones of extension ahead of the tunnel face and in the tunnel walls, which are expected zones of fracturing that could lead to boring problems. These fractured zones will mean that tunnel

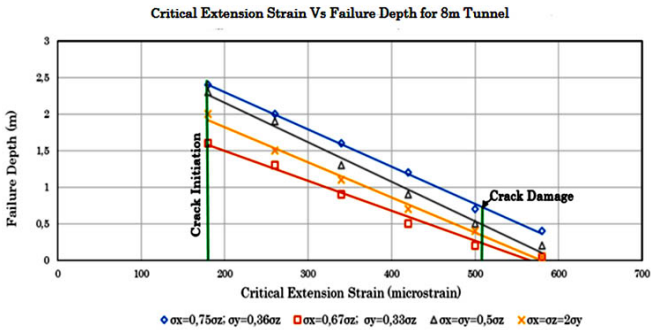

Figure 9—The predicted failure depth for different stress ratios for an 8 m diameter tunnel (Poisson's ratio 0.2)

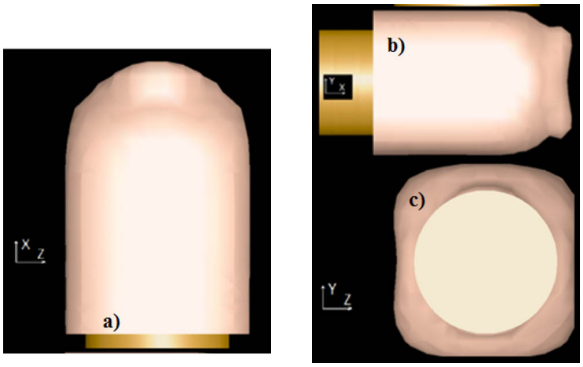

Figure 10—Isosurfaces of fracture/crack initiation for an 8 m diameter tunnel according to extension strain criterion for Poisson's ratio of 0.2: a) top view of the tunnel b) side view of the tunnel c) front view of the tunnel (σ_x= 70MPa, σ_y= 35MPa, σ_z= 70MPa; x-axial; y-vertical; z-horizontal)

faces will be advanced into fractured rock, potentially causing problems with the head and cutters, and fracturing in the walls could lead to their instability, and gripping problems. The distance of predicted fracture development ahead of the face of the tunnel is dependent on the relative magnitudes of the principal stresses, and on the value of Poisson's ratio.

The orientations of extension fractures are normal to the minor principal stress orientation, that is, in the σ_1-σ_2 plane. Using the trajectory ribbon facility in Examine 3D, these orientations can be displayed, as shown in Figure 11. These ribbons illustrate the potential for the formation of 'plates' with flat slab, curved plate, and shell geometries ahead of the face. Buckling of such geometries will result in the release of the energy stored in the 'plate' due to the high stress levels. This release of energy could manifest as spalling and rock bursting, such as reported by Zhang et al. (2012) and Feng et al. (2018). Cutter pressures and their cutting action will also contribute to the break-up of the 'plates' in the absence of stresses sufficiently high to cause buckling.

As indicated in Figure 11, the rock ahead of the tunnel face will be substantially fractured and thus contain many incipient 'plates'. To illustrate the extent of such zones, isosurfaces were generated, assuming a critical extension strain of 200 microstrain, which may be considered to be typical for brittle quartzite (Wesseloo and Stacey, 2000). It is suggested that the observed thickness of such 'plates' may be dictated by their buckling potential, which was thus investigated using three approaches.

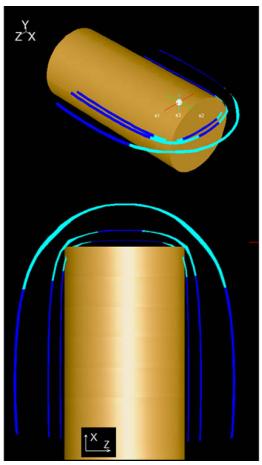

Figure 11—Orientations of fractures around an 8m diameter tunnel (σx=70 MPa, σy=35 MPa and σz=70 MPa)

McGarr (1997) analysed slab buckling in excavation sidewalls, with dimension L, taking the maximum stress in the excavation sidewall (σ) to be close enough to the magnitude of the uniaxial compressive strength (UCS) of the rock, to generate cracks parallel to the free surface. The equation that follows, was used to analyse the generated slabs, with thickness of h, using a UCS of 180 MPa (E: elastic modulus; ν: Poisson's ratio):

$$h/L = \{2\sqrt{3}\sqrt{(1-\upsilon^2)}\sqrt{\frac{\sigma}{E}}\}/\pi$$

$$= \{2\sqrt{3}\sqrt{(1\text{-}0.2^2)}\sqrt{(180/50000)}\}/\pi \quad [3]$$

$$= 0.0648$$

Therefore, the slenderness ratio L/h = 15.43. This is equivalent to l/t in Kazakidis (2002), who used Euler's formula to calculate buckling stress (σ_b):

$$\sigma_b = \pi^2 E/\{12(l/t)^2\}$$

$$= 172.8 \text{ MPa} \quad [4]$$

These values are indications of the critical stress at which slab buckling would take place, and the slenderness ratio of 15.43, below which buckling failure will occur. The amplitude of flexure is given by:

$$C_1 = (2/h)(L/\pi)^2\{(1\text{-}\nu^2)/E\}\sigma_1$$

$$= 0.000664L^2/h \quad [5]$$

Where:

L: Diameter
σ_1: Applied stress
h: Slab thickness
L/h: Slenderness ratio
C_1: Amplitude of flexure

The amplitude of flexure determines the point at which a tensile crack would propagate, causing the slab to break into two parts. It is apparent from the results obtained, that for the specified mechanical properties of rock, the amplitude of flexure will be dependent on the ratio of the square of the slab length to the slab thickness for non-circular excavations.

Similar models to that of McGarr (1997), were generated from the results obtained in Examine 3D, as indicated in Figures 12 and 13. It can be seen that, at the point where possible buckling is expected, the σ_1/σ_3 ratios range from 3.5 to 3.8 for a 6 m diameter tunnel and 3 to 5 for an 8 m diameter tunnel. The afore-mentioned equations were used to calculate some of the important parameters for the analysis of slab buckling. The results are summarized in Tables III and IV. For these values, graphs of generated stress versus slenderness ratio were plotted, shown in Figures 12 and 13, where an average slenderness ratio of 13 is predicted for 180 MPa, as indicated by red arrows on the graphs. It is apparent that the buckling stress is dependent on the slenderness ratio and elastic modulus.

It is evident that the smaller the slenderness ratio, the larger the buckling stress needed for buckling. When comparing the applied stress (σ1) and the buckling stress (σ_b), it can be seen that buckling is predicted. It is worth noting that the slab thicknesses determine the extent of the stability problem, in this case, the boring difficulty. For instance, comparing a 4 m diameter tunnel with an 8 m diameter tunnel, the slab thicknesses predicted are 150 mm and 340 mm, respectively. This implies that, owing to the much greater volume of rock involved, an eight-metre diameter tunnel would cause more boring problems than a four-metre tunnel at the same depth.

Contrary to this, when considering the buckling stress, considering the UCS of the rock, buckling is not predicted. According to Kazakidis (2002), the disadvantage of using Euler's approach is the fact that, as the slenderness ratio increases, the presence of imperfections is likely to increase. Therefore, buckling can still occur, even under low critical loads (P_{cr}). In order to overcome this, the eccentricity of the applied load is considered, where the strength of the material is not taken into consideration. Therefore, the criterion of failure is based on the magnitude of the compressive (σ_{cmax}) and tensile (σ_{tmax}) stresses in the material. The following Equations [6]–[7] are used to calculate these parameters:

$$\sigma_{cmax} = \sigma + 6(\sigma/t)[e/\cos(l\sqrt{(3\sigma/E)/t})] \quad [6]$$

$$\sigma_{tmax} = \sigma - 6(\sigma/t)[e/\cos(l\sqrt{(3\sigma/E)/t})] \quad [7]$$

Application of these formulae yields the results in Tables V and VI, and Figures 14 and 15, assuming eccentricity (e) of t/4. It can be seen that potential buckling can be predicted when the slenderness

Table III

Summary of slab thickness, slenderness ratios and buckling stresses

In Situ Stresses										
σx=70MPa, σy=35 MPa, σz=70 MPa										
Diameter, L(m)	σ3 (MPa)	σ1 (MPa)	h/L	h (m)	l/h	σb (MPa)	σ1/ σ3	C1	σcr	σcomp(MPa)
2	33	70	0,038	0,075	26,316	57,967	2,121	0,03541	43,9277	175,58
4	33	70	0,038	0,15	26,316	57,967	2,121	0,07083	39,5901	175,66
6	28,5	90	0,043	0,255	23,256	74,529	3,158	0,09374	37,2541	226,06
8	15	100	0,045	0,359	22,222	82,810	6,667	0,11837	35,6807	251,34

Table IV

Summary of slab thickness, slenderness ratios, buckling stresses

In Situ Stresses										
σx=35MPa, σy=35 MPa, σz=70 MPa										
Diameter, L(m)	σ3 (MPa)	σ1 (MPa)	h/L	h (m)	l/h	σb (MPa)	σ1/ σ3	C1	σcr(Mpa)	σcomp(MPa)
2	30	65	0,036	0,072	27,778	53,827	2,167	0,03689	43,9287	163
4	31,5	70	0,038	0,15	26,316	57,967	2,222	0,07083	39,5905	175
6	28	80	0,04	0,241	25,000	66,248	2,857	0,09919	37,2543	200
8	30	90	0,043	0,341	23,256	74,529	3,000	0,12462	35,6809	225

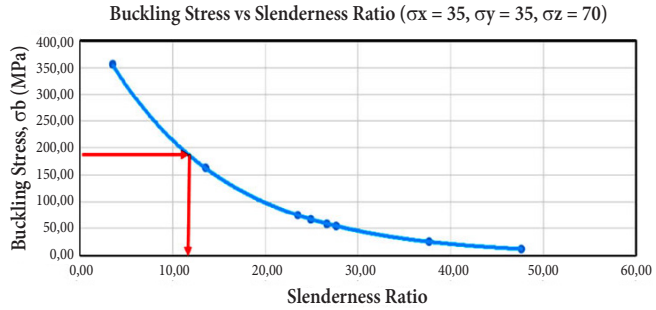

Figure 12—Buckling stress versus slenderness ratio for buckling failure

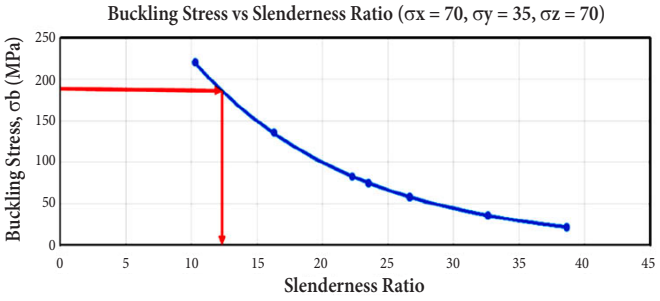

Figure 13—Buckling stress versus slenderness ratio for buckling failure

Table V

Results for eccentric load approach for the determining maximum compressive and tensile stresses for σ_x=35 MPa, σ_y = 35 MPa, σ_z = 70 MPa

D (m)	t (m)	σ (MPa)	l/t	σ^{max}_{compr} (MPa)	σ^{max}_{tens} (MPa)
2	0.075	65	27.64	163	-33
4	0.150	70	26.64	175	-35
6	0.255	80	24.91	200	-40
8	0.359	90	23.49	225	-45

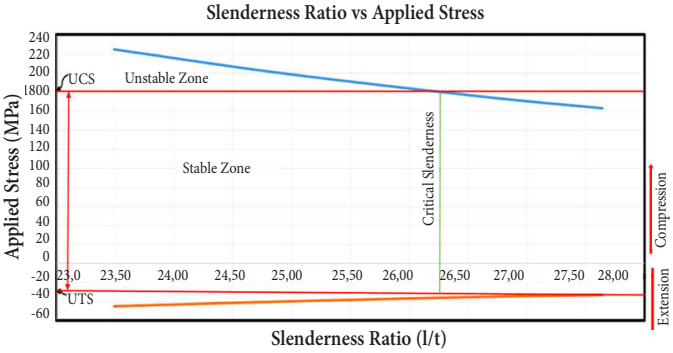

Figure 14—Determination of critical slenderness ratio for buckling analysis under eccentric load

ratio is 26.2 or less, indicating that the compressive strength has been exceeded. This area is indicated as an unstable zone. The zone within the limits of UCS and uniaxial tensile strength (UTS) denotes stability, as can be seen in both Figures 14 and 15.

Conclusions

Observation of rock fracturing behaviour around the face of bored excavations under high stresses indicates the formation of extension fractures in the rock ahead of the face. A series of stress analyses was carried out to determine stress and strain distributions around

Table VI

Results for eccentric load approach for the determining maximum compressive and tensile stresses for σ_x = 70 MPa, σ_y = 35 MPa, σ_z = 70 MPa

D (m)	t (m)	σ (MPa)	l/t	e (t/4)	σcom(MPa)	σtens(MPa)
2,00	0,08	70,00	26,64	0,02	175,58	-35,58
4,00	0,15	70,00	26,64	0,04	175,66	-35,66
6,00	0,26	90,00	23,49	0,07	226,06	-46,06
8,00	0,36	100,00	22,28	0,09	251,34	-51,34

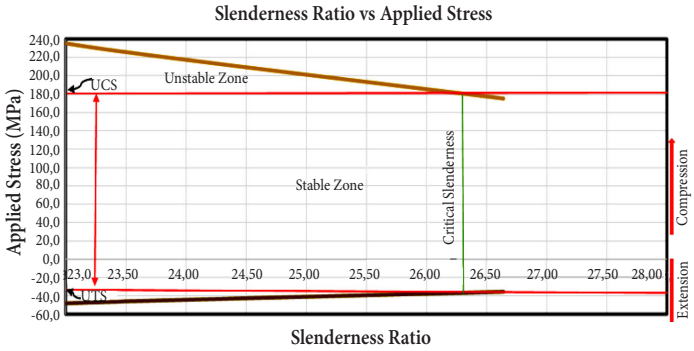

Figure 15—Determination of critical slenderness ratio for buckling analysis under eccentric load

and ahead of the faces of circular tunnels of various dimensions. Using an extension strain fracture criterion, the potential extents of fracturing ahead of the faces were determined, as well as the orientations of the extension fractures. The results of these analyses confirmed the observed fracturing behaviour. Using plate buckling theory, slab thicknesses, and their potential for failure were assessed. Stability was assessed by applying several plate buckling approaches to assess the buckling loads, and minimum and maximum compressive and tensile stresses. As can be expected, the results indicate that tunnels with larger diameters are more prone to significant failures than smaller diameter tunnels.

It is concluded that extension fracturing ahead of bored excavations can lead to the formation of rock slabs, and these can result in two failure mechanisms: slabs can suddenly detach with some violence from the face, and slabs formed may subsequently buckle with violence. Both mechanisms may result in rock bursts. The breaking up of the rock slabs by the cutters or by the bursting will result in blocky rock conditions, which can cause damage to the cutters and head, and lead to poor boring conditions. Damage to borers owing to severe bursting has also been reported.

References

Barla, G. 2014. TBM Tunneling in Deep Underground Excavation in Hard Rock with Spalling Behaviour. *Proc Geomechanik-Kolloquium*, Universitat Freiberg, pp. 25–39.

Barton, N., Shen, B. 2017a. Risk of shear failure and extensional failure around over-stressed excavations in brittle rock. *Journal of Rock Mechanics and Geotechnical Engineering*, (9), pp. 210–225. https://doi.org/10.1016/j.jrmge.2016.11.004

Barton, N., Shen, B. 2017b. Extension failure mechanisms explain failure initiation in deep tunnels and critical heights of cliff faces and near-vertical mountain walls. *American Rock Mechanics Association*, ARMA, vol. 17, no. 686, 20p.

Burgess, H., Taylor, J G. 1980. Tunnel boring in a deep South African gold mine. *Trans. I.M.M., Section A,* April 1980, pp. A84–A98.

Feng, X-T., Xu, H., Qui, S-L., Li, S-J., Yang, C-X., Guo, H-S., Cheng, Y., Gao, Y-H. 2018. In situ observation of rock spalling in the deep tunnels of the China Jinping Underground Laboratory (2400m depth). *Rock Mechanics and Rock Engineering*, vol. 51, pp. 1193–1213.

Gong, Q. M., Yin, L. J., Wu, S. Y., Zhao, J., Ting, Y. 2012. Rock burst and slabbing failure and its influence on TBM excavation at headrace tunnel in Jinping II hydropower station. *Engineering Geology*, vol. 124, pp. 98–108.

Graham, P.C. 1976. Some problems associated with the use of a tunnel boring machine in deep-level mines, in Tunnelling '76, ed. M.J. Jones, *IMM London*, pp. 397–403.

Hadjiabdolmajid, V., Kaiser, P. K., Martin, D. C. 2002. Modelling brittle failure of rock. *International Journal of Rock Mechanics and Mining Sciences*, vol. 39, pp. 731–741.

Hern, G.L., Engelsman, K.I. 1988. Two pass drilling a 6.1-meter diameter ventilation shaft. *Proceedings of the 5th Australia-New Zealand Conference on Geomechanics*. The Institution of Engineering and Technology, Australia, pp. 224–228.

ISRM. 2012. Why does it crack?, ISRM News Journal.

Kaiser, P.K. 2006. Rock mechanics considerations for the construction of deep tunnels in brittle ground, Keynote Lecture, *Asia Rock Mechanics Symposium*, Singapore, 12p

Kaiser, P. K., McCreath, D., Tannant, D. 1996. *Canadian Rock burst Support Handbook*, Sudbury: Geomechanics Research Centre and CAMIRO.

Kazakidis, V.N. 2002. Confinement effect and energy balance analyses for buckling failure under eccentric loading condition. *Rock Mechanics and Rock Engineering*, vol. 35, no. 2, pp. 115–126.

Loew, S., Barla, G., Diederichs, M. 2010. Engineering geology of Alpine tunnels: Past, present and future. *Geologically active—Proceedings of the 11th IAEG Congress*, pp. 201–253.

Martin, C.D. 1997. Seventeenth Canadian Geotechnical Colloquium: The effect of cohesion loss and stress path on brittle rock strength. *Canadian Geotechnical Journal*, vol. 34, no. 5, pp. 698–725.

Martin, C.D., Read, R.S., Martino, J.B. 1997. Observations of brittle failure around a circular test tunnel. *International Journal of Rock Mechanics and Mining Sciences*, vol. 34 no. 7, pp. 1065–1073.

McGarr, A. 1997. A mechanism for high wall-rock velocities in rockbursts. *Pure and Applied Geophysics,* vol. 150, pp. 381–391.

Ortlepp, W. D. 2001. The mechanism of a rock outburst in a quartzite tunnel in a deep mine. *RaSiM5, South African Institute of Mining and Metallurgy*, 5p.

Roberts, D. 2017. Calibration of a numerical model for bore-and-fill mining. *Journal of the Southern African Institute of Mining and Metallurgy*, vol. 117, no. 7, pp. 705–718.

Rojat, F., Labiouse, V., Kaiser, P.K., Descoeudres, F. 2009. Brittle rock failure in the Steg Lateral Adit of the Lotschberg Base Tunnel. *Rock Mechanics and Rock Engineering,* vol. 42, pp. 341–359.

Stacey, T.R. 1982a. Contribution to the mechanism of core discing, *Journal of the Southern African Institute of Mining and Metallurgy*, vol. 82, no. 9, pp. 269–274.

Stacey, T.R. 1982b. Mechanical mining of strong brittle rock by large diameter "Stopecoring" - rock mechanics investigations, *Proceedings of the 14th Canadian Rock Mechanics Symposium*, Vancouver, pp 96–99.

Stacey, T.R. 1981 A simple extension strain criterion for fracture of brittle rock. *International Journal of Rock Mechanics and Mining Sciences*, vol. 18, pp. 469–474.

Stacey, T.R., De Jongh, C.L. 1977. Stress fracturing around a deep level bored tunnel. *Journal of the Southern African Institute of Mining and Metallurgy*, vol. 78, no. 5, pp. 124–133.

Stacey, T.R., Harte, N.D. 1989. Deep level raise boring - prediction of rock problems. *Proceedings of the International Symposium, Rock at Great Depth.* Rock at Great Depth, ed V. Maury & D. Fourmaintraux, A A Balkema, vol. 2, pp. 583–588.

Stacey, T.R., Yathavan, K. 2003. Examples of fracturing of rock at very low stress levels. *Proceedings of the 10th International Society for Rock Mechanics, ISRM 2003 – Technology Roadmap for Rock Mechanics.* The Southern African Institute of Mining and Metallurgy, pp. 1155–1159.

Steffanizzi, S., Barla, G., Kaiser, P.K. 2007. Numerical modelling of strain driven fractures around tunnels in layered rock masses. *Proceedings of the 11th International Congress of the International Society for Rock Mechanics,* Ribeiro, Olalla and Grossmann (eds), Taylor and Francis Group, London, pp. 971–974.

Taylor, J.G., Taylor, R.N., Hall, A.E. 1978. The introduction of a tunnel borer into a South African gold mine. *Journal of the Southern African Institute of Mining and Metallurgy,* vol. 78, pp. 188–198.

Van Aswegen, G. 2013. Forensic rock mechanics, Ortlepp shears and other mining induced structures. *Proceedings of RaSIM 2013, 8th International Symposium on Rockbursts and Seismicity in Mines*, St Petersburg, Russia.

Vazaios, I., Diederichs, M.S., Vlachopoulos, N. 2019a. Assessment of strain bursting in deep tunnelling by using the finite-discrete element method. *Journal of Rock Mechanics and Geotechnical Engineering*, vol. 11, pp. 22–37.

Vazaios, I., Vlachopoulos, N., Diederichs, M.S. 2019b. Assessing fracturing mechanisms and evolution of excavation damaged zone of tunnels in interlocked rock masses at high stresses using a finite-discrete element approach. *Journal of Rock Mechanics and Geotechnical Engineering*, vol. 11, pp. 701–722.

Weh, M., Bertholet, F. 2005. TBM_Vortrieb und spannungsinduzierte Abschalungen im Vortrieb Raron/Steg, Presentation at GEAT'05 Symposium, Zurich, Switzerland, 9p.

Wesseloo, J. 2000. Predicting the extent of fracturing around underground excavations in brittle rock. *Proceedings of the South African Young Geotechnical Engineers Conference*, Stellenbosch. South African Institute of Civil Engineers, 12p.

Wesseloo, J., Stacey, T.R. 2016. Reconsideration of the extension strain criterion. *Rock Mechanics and Rock Engineering*, vol. 49, no. 12, pp. 4667–4679.

Wesseloo, J., Stacey, T.R. 2000. Face and sidewall fracturing in circular excavations and effects on excavation and support. *Proceedings of the ITA World Tunnel Congress, "Tunnels Under Pressure"*, Durban, South Africa, May 2000. The Southern African Institute of Mining and Metallurgy, pp. 553–558.

Xiang, Z., Moon, T., Si, G., Oh, J., Canbulat, I. 2023. Numerical analysis of V-shaped borehole breakout using three-dimensional discrete-element method. *Rock Mechanics and Rock Engineering*, vol. 56, pp. 3197–3214.

Zhang, C., Feng, X-T., Zhou, H., Qiu, S., Wu, W. 2012. Case histories of four extremely intense rockbursts in deep tunnels. *Rock Mechanics and Rock Engineering,* vol. 45, pp. 275–288. ◆